Excellent Mechanical Properties of the Silicate Glasses Modified by CeO2 and TiO2: A New Choice for High-Strength and High-Modulus Glass Fibers

Chao Chen
China Jiliang University - Xiasha Higher Education Campus: China Jiliang University
Qingong Zhu
China Jiliang University - Xiasha Higher Education Campus: China Jiliang University
Huanping Wang
China Jiliang University - Xiasha Higher Education Campus: China Jiliang University
Feifei Huang (huangfeifei.88@163.com)
China Jiliang University - Xiasha Higher Education Campus: China Jiliang University
Qinghua Yang
China Jiliang University - Xiasha Higher Education Campus: China Jiliang University
Shiqing Xu
China Jiliang University - Xiasha Higher Education Campus: China Jiliang University

Research Article

Keywords: SiO2-Al2O3-MgO glasses, TiO2, CeO2, Mechanical properties

Posted Date: March 31st, 2021

DOI: https://doi.org/10.21203/rs.3.rs-346561/v1

Excellent mechanical properties of the silicate glasses modified by CeO_2 and TiO_2: a new choice for high-strength and high-modulus glass fibers

Chao Chen[1], Qingong Zhu[1], Huanping Wang[1*], Feifei Huang[1*], Qinghua Yang[1], Shiqing Xu[1]

[1]Institute of Optoelectronic Materials and Devices, China Jiliang University, Hangzhou, 310018, China

*Corresponding author: wanghuanping@cjlu.edu.cn&huangfeifei.88@163.com

Abstract: As is well known, silicate glass has a stable glass-forming region and mature drawing processes into fibers. In this study, to obtain enhanced mechanical properties, glasses with a composition of SiO_2-Al_2O_3-MgO-CaO-B_2O_3-Fe_2O_3 were synthesized using TiO_2 and CeO_2. When the amount of TiO_2 and CeO_2 is less than 2 wt%, the mechanical properties increase with increases in the TiO_2 and CeO_2. However, as the amount of TiO_2 and CeO_2 increases from 2 to 3.5 wt%, the mechanical properties decrease. Co-doping with 1 wt% TiO_2 and 1 wt% CeO_2 was found to be the optimum approach, with a density, bending strength, compression strength, and compression modulus of 2.626 g/cm^3, 108.36 MPa, 240.18 MPa, and 115.03 GPa, respectively. The optical band gap and Raman spectroscopy proved that, as long as the content of oxygen bonds reaches the maximum level, a kind of best structural stability and mechanical properties will be achieved. Hence, this type of high-strength silicate glass can be used in optical fibers for military defense, wind power generation, and transportation.

Keywords: SiO_2-Al_2O_3-MgO glasses; TiO_2; CeO_2; Mechanical properties

1. Introduction

During the recent decades, high-strength-modulus glass fibers have been widely used in aerospace, military defense, wind power generation, transportation, and sports, among other applications [1–3]. Currently, SiO_2-Al_2O_3-MgO glass fibers, which are high in tensile strength, elastic modulus, and impact resistance, among similar products, have received increased attention in the global manufacturing market [4–7]. However, few recent studies have reported the influence of the composition on the mechanical properties of SiO_2-Al_2O_3-MgO glass, let alone the influence of different additives on the mechanical properties of such glass.

The mechanical properties of glass fibers are in close contact with the different additives in the glasses. In order to improve performance, appropriate stabilizers such as rare earth oxides and transition metals are usually introduced into the glass matrix. [8, 9], among which CeO_2 is a typical case. Similar to Al_2O_3-B_2O_3-SiO_2 glasses doped with CeO_2, the network structure is improved as the amount of CeO_2 increases at under 0.4 mol% [10]. It was also found that the number of bridging oxygen bonds are generated in aluminosilicate glass at a doped molar concentration of 3.5% CeO_2 and CeF_3, achieving the maximal thermal stability [11]. Cerium presents two different valence states: Ce^{4+} and Ce^{3+}, due to a ceric-cerous redox equilibrium in a glass structure. A moderate amount of Ce^{4+} inside the glass can avoid the trapping of electrons produced through a reaction and absorb free electrons, thereby obstructing the formation of permanent defect centers and improving the properties of the glass [12, 13].

In addition, an excessive amount of CeO_2 will produce a series of crystallizations as well as non-bridging oxygen, thereby inducing a negative effect on the mechanical properties and drawing process of the glass. It is therefore necessary to add an oxide to make up for the defects of CeO_2. The valence states of titanium result in TiO_2 playing an important role in the structural properties of glass, suppressing the reduction of Ce^{4+} into Ce^{3+} as well as a decrease in the amount of free oxygen, thereby increasing the chemical and mechanical properties [14]. Moreover, it has been suggested that, in a combined incorporation of the cerium and titanium oxides in Li_2O-Bi_2O_3-SiO_2 and Na_2O-Bi_2O_3-P_2O_5 glass, a proper mixing can significantly improve the mechanical properties [15–17].

According to the relatively outstanding properties of SiO_2-Al_2O_3-MgO glass and excellent characterization of TiO_2 and CeO_2, the effects of TiO_2 and CeO_2 doping on the mechanical properties of SiO_2-Al_2O_3-MgO glass when changing the amounts of TiO_2 and CeO_2 are discussed herein.

2. Experimental procedure

2.1 Sample preparation

Based on our previous study, we prepared 10 samples with mass concentrations of 61 wt% SiO_2-9 wt% Al_2O_3-24 wt% MgO-5 wt% CaO-0.9 wt% B_2O_3-0.1 wt% Fe_2O_3 doped with x wt% TiO_2-y wt% CeO_2 (x = 0, 0.5, 1, 1.5, and 2; y = 0, 0.5, 1, 1.5, and 2), high-purity SiO_2, Al_2O_3, MgO, CaO, B_2O_3, Fe_2O_3, TiO_2, and CeO_2 powders were used in the experimental processes as shown in Table 1. The starting powders were heated at 1650 °C for 5 h in pure silica crucible until it melts. Pour the melts onto a steel plate which is preheated at 500°C and then annealed for 2 h at approximately 850 °C to remove mechanical stress inside glass. The annealed glass is cooled in the furnace at 25°C. Finally, all as-prepared samples were cut into a size of 30.00 mm × 3.00 mm × 3.00 mm (strips) and 10.00 mm × 10.00 mm × 2.00 mm (flakes), which were optically polished prior to measurement.

2.2 XRD measurements

To confirm the amorphous state of the glass sample, an X-ray diffraction (XRD) analysis was used. The XRD spectra were recorded within a Bragg angle 2θ of 10° to 70° in a diffractometer (D2 PHASER) using Cu radiation with a scanning speed of 0.05° per second.

2.3 Raman spectra and optical band gap

The Raman measurement was performed using the 785 nm line of a Renishaw high-power diode laser as the excitation source working at 1.0 W. The measurement was conducted using a DILOR XY triple spectrometer equipped with the 1800 g/mm holographic grating and a CCD detector, using liquid N_2 cooling. The measurement was performed under an Olympus microscope with backscattering geometry, and the glass was recorded at room temperature using a fiber-optic UV-visible spectrometer (model AVASPEC 3648) within the range of 200-800 nm. Glass's absorption of ultraviolet and visible light excites oxide ions to higher energy levels. The absorption coefficient is derived from the formula. (1) [18] can be used to calculate the optical band gap as a function of the wavelength in the ultraviolet-visible spectral range. The optical band gap reflects the structural information of the glass network, where α, T and t are absorption coefficients, transmittance (%) and glass thickness

$$\alpha = \frac{-\ln T}{t} \tag{1}$$

The amorphous material model proposed by Mott and Davis quantitatively correlates the linear absorption coefficient α with the incident photon energy E, as shown in Eq. (2) [19, 20], so the photon energy E is equal to ch/λ, where B, E_{opt}, c, λ and h are constants, and the optical band gap, light speed, wavelength and slab constant are respectively.

$$\alpha E = B(E - E_{opt})^{1/2} \tag{2}$$

The transformation of Eq. (2) A linear relationship between α and hc/λ is generated, and the optical band gap E_{opt} is estimated by using the intercept on the horizontal axis by extrapolating the linear graph to the zero coordinate.

2.4 Characterization of mechanical properties

At room temperature, a sensitive microbalance using deionized water as the immersion liquid uses the standard Archimedes principle to measure the density of glass samples. The molar oxygen packing density (*OPD*) is calculated using Eq. (3) [21], where ρ, M and C are the density, average molecular weight and number of oxygen molecules of each formula unit respectively.

$$OPD = 1000C\left(\frac{\rho}{M}\right) \tag{3}$$

Then use the WDW-2E universal testing machine to measure the bending strength. The results of the bending strength experiments can be calculated using Eq. (4) [22, 23], where L, b, t, F, and B, respectively, are the length, width, thickness, yield stress, and bending strength of the samples.

$$B = \frac{3FL}{2bt^2} \tag{4}$$

In addition, the compression modulus was measured using a CMT5105 electromechanical universal testing machine, and calculated through Eqs. (5) and (6) [24], where b, t, F, σ, ε, and E_c are the width, thickness, yield stress, compression strength, strain, and compression modulus of the samples, respectively.

$$\sigma = \frac{F}{bt^2} \tag{5}$$

$$E_c = \frac{\sigma}{\varepsilon} \tag{6}$$

Various factors such as multiple internal transmittances of the transducer and microcracks on the sample surface may affect the accuracy of ultrasonic mechanical performance indicators. Therefore, all glass samples were polished with SiC paper at up to 1200 grit, and then ultrasonically cleaned with distilled water to ensure uniform parallelism, flatness and smoothness. The average of the six samples is used as the result of the above test.

In order to quantitatively evaluate the deviation, the error based on the standard deviation reflects the error of bending strength, compressive strength and compressive modulus. The equation is expressed as follows [25, 26]:

$$\sigma = \sqrt{\frac{1}{N-1}\sum_{i=1}^{N}(Xi - \overline{X})^2} \tag{7}$$

3 Results and discussion

3.1 Phase structure analysis

Some correlation theories show that the additives may destroy the internal structure of the glass and affect its structural stability, particularly TiO_2, CeO_2, and Y_2O_3. These metal and rare earth oxides have large ionic radii and electron densities, which may lead to crystallization, decreasing the mechanical properties of the glass after drawing [27, 28]. Therefore, to judge whether glass doped with TiO_2 and CeO_2 shows an interior crystallization, the XRD patterns of the glass are used, as shown in Fig. 1. Such patterns reveal that combing undoped TiO_2 with CeO_2 glass (SAM-1) does not result in an evident crystallization peak for the other samples, thereby proving that the addition of TiO_2 and CeO_2 will not adversely induce crystallization.

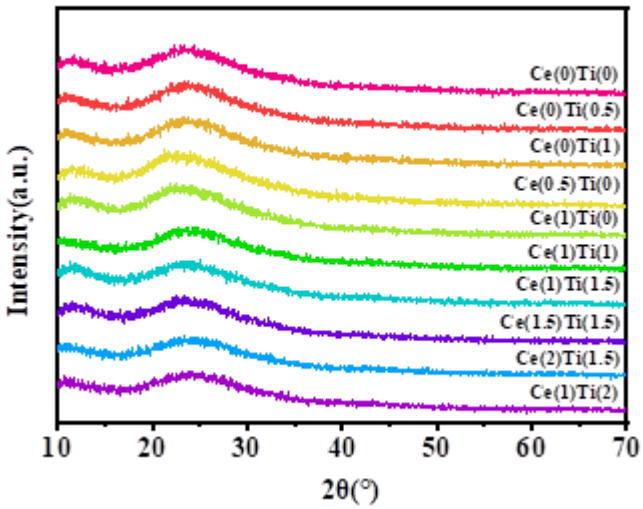

Fig. 1. XRD patterns of glass doped with different amounts of TiO_2 and CeO_2

Table 1. Chemical composition of glass (wt/%)

Sample	SiO_2-Al_2O_3-MgO system glasses						CeO_2	TiO_2
	SiO_2	Al_2O_3	MgO	CaO	B_2O_3	Fe_2O_3		
SAM-1	61	18	15	5	0.9	0.1	0	0
SAM-2	61	18	15	5	0.9	0.1	0	0.5
SAM-3	61	18	15	5	0.9	0.1	0	1
SAM-4	61	18	15	5	0.9	0.1	0.5	0
SAM-5	61	18	15	5	0.9	0.1	1	0
SAM-6	61	18	15	5	0.9	0.1	1	1
SAM-7	61	18	15	5	0.9	0.1	1	1.5
SAM-8	61	18	15	5	0.9	0.1	1.5	1.5
SAM-9	61	18	15	5	0.9	0.1	2	1.5
SAM-10	61	18	15	5	0.9	0.1	1	2

3.2 Raman spectra and optical band gap

In the Raman spectra of glass at room temperature, as shown in Fig. 2, dominating peaks at approximately

950 and 1150 cm^{-1} can be seen in all compositions. The antisymmetric vibration of Si-O_{nb} produces a strong and wide frequency band at 950 cm^{-1}, while the symmetrical tensile vibration of Si-O-Si produces a high frequency band at about 1150 cm^{-1}, both of which characterize the number of oxygen bonds within the glass [29, 30]. In addition, the internal bridge of oxygen bonds can indicate the stability of the silicate glass [31]. When the amounts of CeO_2 and TiO_2 range from 0 wt% to 2 wt%, as the intensities of the anti-symmetric vibrations of Si-O_{nb} and the symmetric stretching vibrations of Si-O-Si increase with the amounts of CeO_2 and TiO_2, the number of bridging oxygen bonds in the glass continuously increases and the peak intensity at 950 and 1150 cm^{-1} of SAM-6 reaches the maximum value, resulting in an enhanced network structure of the glass. Meanwhile, because the amounts of CeO_2 and TiO_2 are greater than 2 wt%, the network structure of the glass becomes inferior owing to the rapid decrease in the Raman intensity.

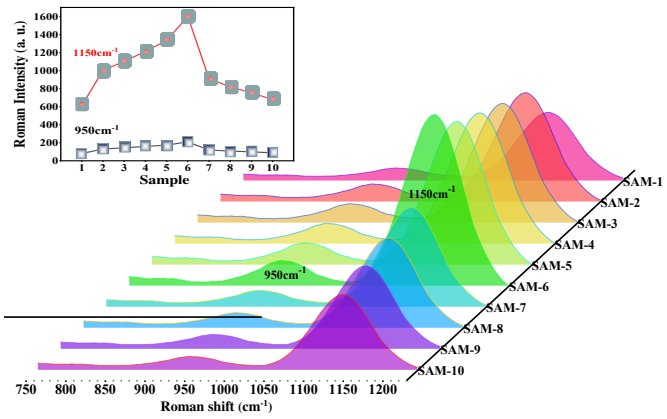

Fig. 2. Raman spectra of glass doped with different amounts of TiO_2 and CeO_2. The illustration shows the positional changes of the two main peaks.

The transmission spectra of different glass components are shown in Fig 3(a). According to the result of Fig 3(a), a linear fitting graph of the transmittance spectra is characterized in Fig. 3(b), and the values of the cut-off wavelength and the optical band gap values (E_{opt}) of the glass are shown in Fig. 3(c). From Fig. 3(c), E_{opt} decreases with increases in TiO_2 and CeO_2 when their amounts are less than 2 wt%, whereas it increases when their amounts increase from 2 wt% to 2.5 wt%. When the amounts of TiO_2 and CeO_2 are 2 wt%, SAM-6 has the minimum optical band gap at 4.38 eV. These results are consistent with the results of the Raman spectra shown in Fig. 2. In general, in a silicate glass system, a lower E_{opt} indicates a more compact network structure of the glass [32, 33]. In addition, TiO_2 and CeO_2 change the number of bridge bonds, thereby changing the optical band gap of the glass. Moreover, CeO_2 and TiO_2 coexist in the glass thermodynamically for a redox reaction, as shown in Eq. (8) [34].

$$2CeO_2 + Ti_2O_3 = 2TiO_2 + Ce_2O_3 \ \Delta G_{1773K} = -71.78 KJ/mol \quad (8)$$

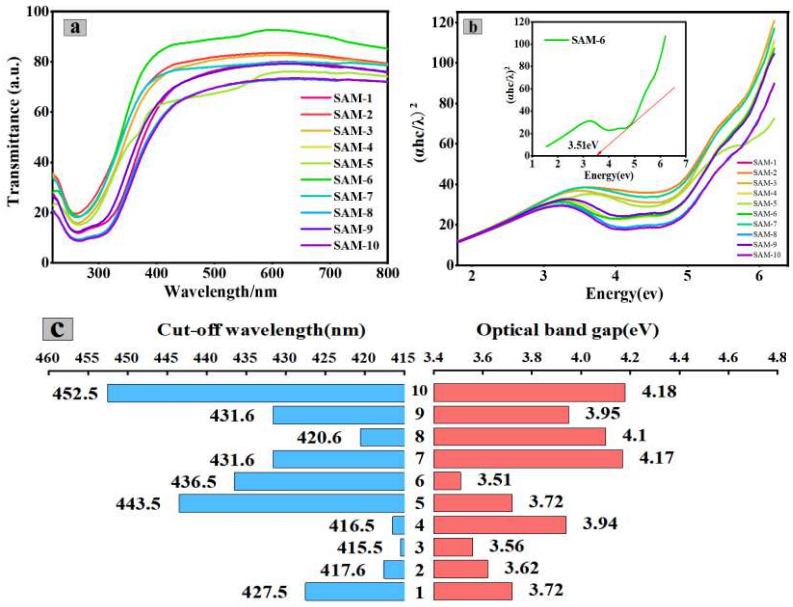

Fig. 3. (a) Optical transmittance of glass doped with different amounts of TiO_2 and CeO_2, (b) linear fitting graph of different samples doped with TiO_2 and CeO_2, and (c) cut-off wavelength of optical band gap of glass doped with different amounts of TiO_2 and CeO_2.

Fig. 4 shows examples of X-ray photoelectron spectroscopy (XPS). For the Ce(0)Ti(0.5) sample, minor peaks observed at 457.1-457.9 and 461.5-462.8 eV are related to Ti^{3+} [35]. With increases in the amounts of CeO_2 and TiO_2, major peaks observed at 459.1-459.3 and 464.8-465.0 are assigned to Ti^{4+}, which indicates that Ti^{3+} will react to generate a large amount of Ti^{4+}, and tetrahedral Ti-O can enter the Si-O network, enhance the interconnectivity of structural units. In this case, the expanded network opening due to the severe deformation of the $[SiO_4]$ tetrahedron is related to the large amount of $[TiO_4]$ and the charge balance between the substitution of Al and Si in the octahedral sites and thesubstitution of Si by Al in the tetrahedral sites, which simultaneously facilitates the entering of $[AlO_4]$ into network [36]. This further increases the number of bridge oxygen bonds, thus increasing the degree of structural cross-linking of the glass. However, the increases in the cerium and titanium concentrations sequentially carry off a large number of bridge oxygen bonds, as shown in Eq. (9) [37].

$$CeO_2 \overset{\Delta}{\leftrightarrow} Ce_2O_3 + [O]\uparrow \tag{9}$$

However, with increases in the amounts of TiO_2 and CeO_2, an excessive amount of $[TiO_4]$ will reduce the proportion of $[SiO_4]$, gradually reduce the degree of polymerization, and increase the optical band gap values, thus decreasing the structural stability of the glass.

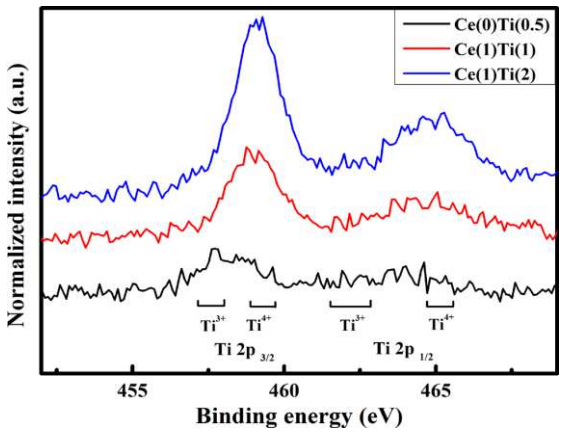

Fig. 4 XPS profiles of representative glasses doped with different amounts of TiO_2 and CeO_2

3.3 Volume density and oxygen packing density

Based on Table 2, the volume and oxygen packing densities of the different glasses are shown in Fig. 5. It can be inferred from Fig. 5 that the volume and oxygen packing densities vary from 2.401 to 2.626 g/cm^3 and 73.423 to 78.725 mol/l, respectively. Among all glass samples, SAM-6 has maximum values of 2.626 g/cm^3 and 78.725 mol/l, individually. The results of these two variables indicate show a similar trend in which both the volume and oxygen packing densities increase with an increase in the amounts of TiO_2 and CeO_2 when the content is less than 2 wt%, whereas a continuous decrease occurs when the content is higher than 2 wt%. As shown in Figs. 2 and 3(c), the Raman intensity increases and the optical band gap decreases as the amounts of TiO_2 and CeO_2 increase from 0 wt% to 2 wt%, which indicates that there are numerous bridging oxygen bonds improving the interconnectivity of the network structure, Therefore, the volume and oxygen filling density are affected. When the content of TiO_2 and CeO_2 is greater than 2.0 wt%, excessive Ti^{4+} and Ce^{4+} will generate redundant non-bridging oxygen bonds in the glass, which destroying the network structure, thereby reducing the volume and oxygen packing density.

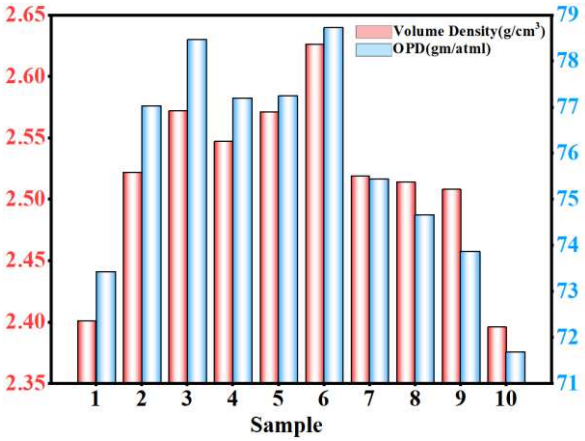

Fig. 5. Volume and oxygen packing densities of glass doped with different amounts of TiO_2 and CeO_2

Table 2. Volume and oxygen packing densities of the glass

Sample	C (number)	M (g/mol)	Volume density ρ (g/cm3)	OPD (mol/l)
SAM-1	1.807	59.090	2.401±0.009	73.423
SAM-2	1.817	59.489	2.522±0.017	77.030
SAM-3	1.827	59.889	2.572±0.013	78.463
SAM-4	1.817	59.951	2.547±0.014	77.195
SAM-5	1.827	60.811	2.571±0.019	77.243
SAM-6	1.847	61.610	2.626±0.022	78.725
SAM-7	1.857	62.009	2.519±0.013	75.437
SAM-8	1.867	62.870	2.514±0.018	74.656
SAM-9	1.877	63.730	2.508±0.012	73.867
SAM-10	1.867	62.409	2.396±0.015	71.678

3.4 Mechanical properties

Table 3 and Fig. 6(a) show the bending strength of glass doped with different amounts of TiO_2 and CeO_2. It can be seen that SAM-6 achieves the maximum bending strength at 108.36 Mpa. Meanwhile, the bending strength increases with increases in the amounts of TiO_2 and CeO_2 of less than 2 wt% because both the Raman intensity and the oxygen packing density increase with increasing amounts of TiO_2 and CeO_2, which indicates the presence of numerous bridge oxygen bonds inside the glass, thus improving the bending strength. However, a moderate amount of Ce^{4+} results in a large attraction, which can increase the bond strength between the metal cations and oxygen ions in the glass and enhance the binding force of the ionic bond, thus improving the bending strength [37, 38]. In addition, when there is enough oxygen, there can be an appropriate amount of Ti^{4+} in the tetrahedral structure, which is beneficial to the interconnection of the network structure, thereby improving the bending strength of the glass [36]. However, as the amount of TiO_2 and CeO_2 increases from 2 to 3.5 wt%, the bending strength decreases. In this context, an excessive amount of CeO_2 will generate more free oxygen, as shown in Eq. (8), resulting in an excessive number of non-bridging oxygen bonds. Meanwhile, the presence of trivalent cerium makes it difficult to bond with four-coordinated Ti-O units according to Pauling rules, and thus the titanium may act as a network intermediate. However, an increase in TiO_2 may result in an increase in non-bridge and bond defects. This then depolymerizes the network by breaking up the Si-O bonds, which induces an increase in the number of microcracks and pores. The structure is unable to resist the external pressure and thus reduces the bending strength of the glass [39].

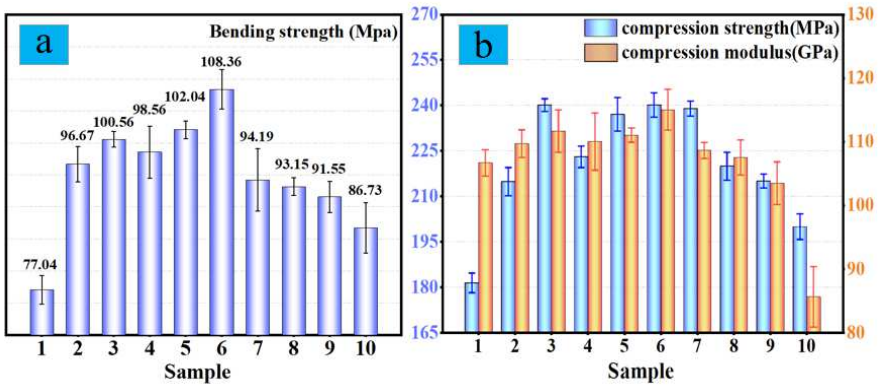

Fig. 6 (a) The bending strength of glass doped with different amounts of TiO_2 and CeO_2, and (b) the compressive strength and modulus of glass doped with different amounts of TiO_2 and CeO_2

Table 3 Bending strength, compression strength, and compression modulus of the glass

Sample	Bending strength (MPa)	Compression strength (MPa)	Compression modulus (GPa)
SAM-1	77.04±2.21	181.49±3.24	106.70±2.06
SAM-2	96.67±2.75	214.88±4.65	109.71±2.19
SAM-3	100.56±1.23	240.15±2.07	111.71±3.33
SAM-4	98.56±4.05	223.11±3.56	110.05±4.48
SAM-5	102.04±1.36	237.10±5.49	111.06±1.13
SAM-6	108.36±3.07	240.21±4.01	115.06±3.20
SAM-7	94.19±4.88	231.99±2.46	108.66±1.26
SAM-8	93.15±1.38	219.69±4.60	107.53±2.75
SAM-9	91.55±2.45	215.05±2.29	103.51±3.35
SAM-10	86.73±3.96	200.00±4.21	85.67±4.76

The compressive strength and modulus of glass doped with different amounts of TiO_2 and CeO_2 are shown in Table 3 and Fig. 6(b). It can be seen that SAM-6 possesses the maximum compression strength and compression modulus of 240.21 MPa and 115.06 GPa, respectively. Meanwhile, the compression strength and compression modulus increase with increasing amounts of CeO_2 and TiO_2, which range from 0 wt% to 2 wt%, when the decreases in the amounts of CeO_2 and TiO_2 are more than 2 wt%. The above laws are clearly consistent with the bending strength of the glass.

4. Conclusions

The influence of TiO_2 and CeO_2 on the mechanical properties of 61 wt% SiO_2-9 wt% Al_2O_3-24 wt% MgO-5 wt% CaO-0.9 wt% B_2O_3-0.1 wt% Fe_2O_3-*x* wt% TiO_2-*y* wt% CeO_2 glass was investigated. When the amounts of TiO_2 and CeO_2 are less than 2 wt%, the Raman intensity increases and the optical band gap decreases when their amounts increase. This can be attributed to the oxidation of Ti^{3+} to Ti^{4+}, which increases the numbers of bridge oxygen bonds, improving the volume intensity, oxygen packing density, bending strength, compression strength, and compression modulus. However, as the amounts of TiO_2 and CeO_2 increase from 2 to 3.5 wt%, an excessive amount of TiO_2 may act as a network intermediate inducing a weakening of the network structure. The bending

strength, compression strength, and compression modulus thereby decrease, and the optical band gap increases. The optimum amounts of TiO_2 and CeO_2 were both found to be 1 wt%, resulting in the largest Raman intensity and the lowest optical band gap, which proves that when the number of epoxy- reaches the maximum, the best glass structure will be achieved. When doped with 1 wt% TiO_2 and 1 wt% CeO_2, the density, bending strength, compression strength, and compression modulus of the derived glass reach 2.626 g/cm^3, 108.36 MPa, 240.18 MPa, and 115.03 GPa, respectively.

Funding statement: This work was supported by the National Natural Science Foundation of China (NSFC) (61975193).

Author Contributions: All of the authors contributed to the idea, simulation of the research, the analysis of the results, and the writing of the manuscript.

Availability of date and material: Not applicable.

Compliance with ethical standards: The authors declare that they have no conflict of interest.

Consent to Participate: Not applicable.

Consent for Publication: Not applicable.

Acknowledgment: Not applicable.

References

[1] G. Pisano, G.R. Carfagni, The statistical interpretation of the strength of float glass for structural applications, J. Constr. bul. Mater. 98 (2015) 741-756.

[2] C. Feng, Lihua Gao, The effects of MgO/Al_2O_3 ratio on viscous behaviors and structures of MgO-Al_2O_3-TiO_2-CaO-SiO_2 slag systems with high TiO_2 content and low CaO/SiO_2 ratio, Trans. J. Nonferrous Met. Soc. 30 (2020) 800-811.

[3] Z. Wang, J. Sun, L. Liu, J. M.Fiber Compos. 4 (2010) 8-10.

[4] N. Nowak, T. Cardinal, F. Adamietz, M. Dussauze, Influence of niobium and titanium introduction on optical and physical properties of silicate glasses, J. Mater. Res. Bull. 48 (2013) 1376-1380.

[5] Shuai Zhang, Yanling Zhang, Zhenmin Qu, Effects of soluble Cr_2O_3 doping on the glass structure, microstructure, crystallization behavior, and properties of MgO-Al_2O_3-SiO_2 sapphirine glass ceramics, J. Mater. Chem. Phys. 252 (2020) 123115.

[6] T. Y. Wei, Y. Hu, L. G. Hwa, Structure and elastic properties of low-temperature sealing phosphate glasses, J. Non-Cryst. Solids. 288 (2001) 140-147.

[7] C.Y. Wang, G.Q. Hu, Z.J. Zhang, B.Q. Liu, Preparation and characterization of Bi_2O_3-SiO_2-Al_2O_3 based glasses of good transparency with high Bi_2O_3 content, J. Non-Cryst. Solids. 363 (2013) 84-88.

[8] C. Zuo, Z. Zhou, L. Zhu, Y. Chen, Effect of CeO_2 on the viscosity and structure of high-temperature melt of the CaO-SiO_2(-Al_2O_3)-CeO_2 system, J. Mater. Res. Bul. 83 (2016) 155-159.

[9] G. Lakshminarayana, E.M. Weis, B.L. Bennett, D.J. Williams, Structural, thermal, and luminescence properties of cerium-fluoride-rich oxyfluoride glasses, J. Opt. Mater. 35 (2012) 117-125.

[10] Zhenlin Wang,Yang Zhaob, Chunyan Zhang, Comparative investigation on the structure and physical properties of CeO_2/TiO_2/Sb_2O_3-doped bismuth borosilicate glasses, J. Non-Cryst. Solids. 544 (2020) 120190

[11] O. Sanz, E. Haro, J. Gonzalo, Influence of the melting conditions of heavy metal oxide glasses containing bismuth oxide on their optical absorption, J. Non-Cryst. Solids. 352 (2006) 761-768.

[12] Y. Sheng, L. Yang, H. Luan, Y. Yu, Evidence of the coexistence of multivalence cerium oxide nano-particles in a sodium borate glass, J. Nucl. Mater, 427 (2012) 58-61.

[13] J.L. Rygel, C.G. Pantano, Synthesis and properties of cerium aluminosilicophosphate glasses, J. Non-Cryst. Solids. 355 (2009) 2622-2629.

[14] G.P.Singh, P.Kaur,S.Kaur,Conversion of covalent to ionic character of V_2O_5-CeO_2-PbO-B_2O_3 glasses for solid state ionic devices, J. Phys. B. 407 (2012) 4168-4172.

[15] Singh K, M. Solid State Ionics. 93 (1996) 147-158.

[16] S. Daviero, L. Montagne, G. Palavit, EXAFS, XANES and 31P double-quantum MAS-NMR of (50-x/2)Na_2O-xBi_2O_3-(50-x/2)P_2O_5 glasses, J. Phys. Chem. Solids. 64 (2003) 253-260.

[17] R. Gao, H.P. Wang and Q.G. Zhu, The forming region and mechanical properties of SiO_2-Al_2O_3-MgO glasses, J. Non-Cryst. Solids. 470 (2017) 132-137.

[18] Jing Wang, Jin-shu Cheng, Zhen-lu Deng, Effect of alkali metal Oxides on viscosity and crystallization of the MgO-Al_2O_3-SiO_2 glasses, Physica B. 415 (2013) 34-37.

[19] M.S. Shakeri, M. Rezvani, Optical band gap and spectroscopic study of lithium alumino silicate glass containing Y^{3+} ions, J. Spectrochim. Acta, part A. 79 (2011) 1920-1925.

[20] D.D. Ramteke, R.S. Gedam, Luminescence properties of Gd^{3+} containing glasses for ultra-violet (UV) light, J. rare earths. 32 (2014) 389-393.

[21] T. Smyth, J. Am. Ceram. Soc. 42 (1959) 277-278.

[22] J. Kameda, T.E. Bloomer, Kinetics of grain-boundary segregation and desegregation of sulfur and phosphorus during post-irradiation annealing, J. Acta Mater. 47 (1999) 893-903.

[23] D. Li, W. Li, R. Wang, X. Shen, Temperature dependence of the three-point bending fracture behavior of soda-lime-silica glass with surface scratch, J. Non-Cryst. Solids. 409 (2015) 126-130.

[24] Y.Z. Zhao, H.R. Yin, Glass Technology. Text. Edu. 7 (2006) 98-100.

[25] B. Pan and Z.X. Lu, Mean intensity gradient: An effective global parameter for quality assessment of the speckle patterns used in digital image correlation, J. Opt. Laser. Eng. 48 (2010) 469-477.

[26] Y. Su and Q.C. Zhang, Quality assessment of speckle patterns for DIC by consideration of both systematic errors and random errors, J. Opt. Laser. Eng. 86 (2016) 132-142.

[27] O. Yasin Keskin, Ramazan Dalmis, Isil Birlik, Comparison of the effect of non-metal and rare-earth element doping on structural and optical properties of CuO/TiO_2 one-dimensional photonic crystals, J. Alloys Compd. 817 (2020) 153262.

[28] Zhenlin Wang, Linqiao Gan, Weijiu Huang, Structural recovery and optical properties stabilization of CeO_2/TiO_2-doped boroaluminosilicate glass under gamma irradiation, J. Radiat Phys Chem. 151 (2018) 133-140.

[29] Guojun Gao, Lili Hu, Huiyan Fan, Effect of Bi_2O_3 on physical, optical and structural properties of boron silicon bismuthate glasses, J. Opt. Mater. 32 (2009) 159-163

[30] T.Y. Wei, Y. Hu, L.G. Hwa, Structure and elastic properties of low-temperature sealing phosphate glasses, J. Non-Cryst. Solids. 288 (2001) 140-147.

[31] H.W. Nesbitt, Grant S. Henderson, G. Michael Bancroft, Bridging oxygen speciation and free oxygen(O^{2-}) in K-silicate glasses: Implications for spectroscopic studies and glass structure, J. Chem. Geol. 461(2017)13-22.

[32] J.L. Rygel, C.G. Pantano, Synthesis and properties of cerium aluminosilicophosphate glasses, J. Non-Cryst. Solids. 355 (2009) 2622-2629.

[33] N. Berwal, R.S. kundu, K. Nanda, N. Kishore, Raman spectra and optical band gap in some PbO-ZnO-TeO_2 glasses, J. mol. struct. 1097 (2015) 37-44.

[34] Jing Wang, Jin-shu Cheng, Zhen-lu Deng, Effect of alkali metal Oxides on viscosity and crystallization of the MgO-Al_2O_3-SiO_2 glasses, J. Physica B. 415 (2013) 34-37.

[35] C.L. Qin, J.J. Oak and N. Ohtsu, XPS study on the surface films of a newly designed Ni-free Ti-based bulk metallic glass, J. Acta. Metall. 55 (2007) 2057-2063.

[36] J. Kameda, T.E. Bloomer, Kinetics of grain-boundary segregation and desegregation of sulfur and

phosphorus during post-irradiation annealing, J. Acta Mater. 47 (1999) 893-903.
[37] E.E. Trusova, N.M. Bobkova, V.S. Gurin, M. Glass Ceram. 66 (2009) 240-244.
[38] V.K. Deshpande, R.N. Taikar, Effect of cerium oxide addition on electrical and physical properties of alkali borosilicate glasses, J. Mater. Sci. Eng. B. 172 (2010) 6-8.
[39] S. Singh, G. Kalia, K. Singh, Effect of intermediate oxide (Y_2O_3) on thermal, structural and optical properties of lithium borosilicate glasses, J. mol. Struct. 1086 (2015) 239-245.

Figures

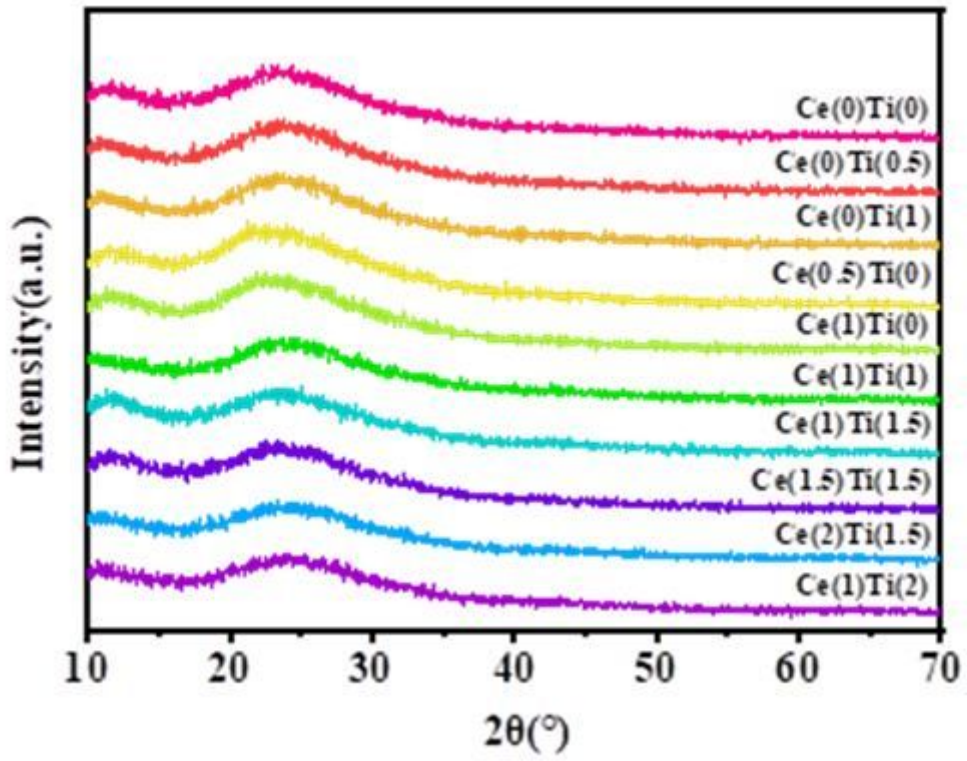

Figure 1

XRD patterns of glass doped with different amounts of TiO2 and CeO2

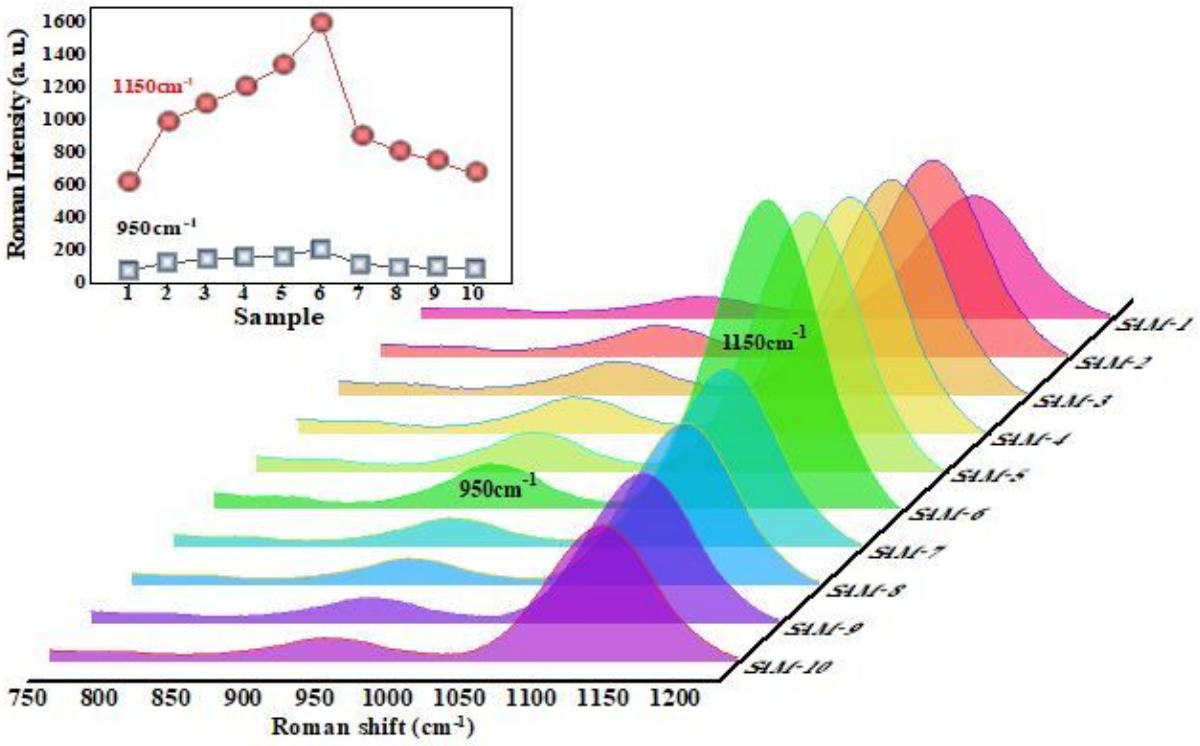

Figure 2

Raman spectra of glass doped with different amounts of TiO2 and CeO2. The illustration shows the positional changes of the two main peaks.

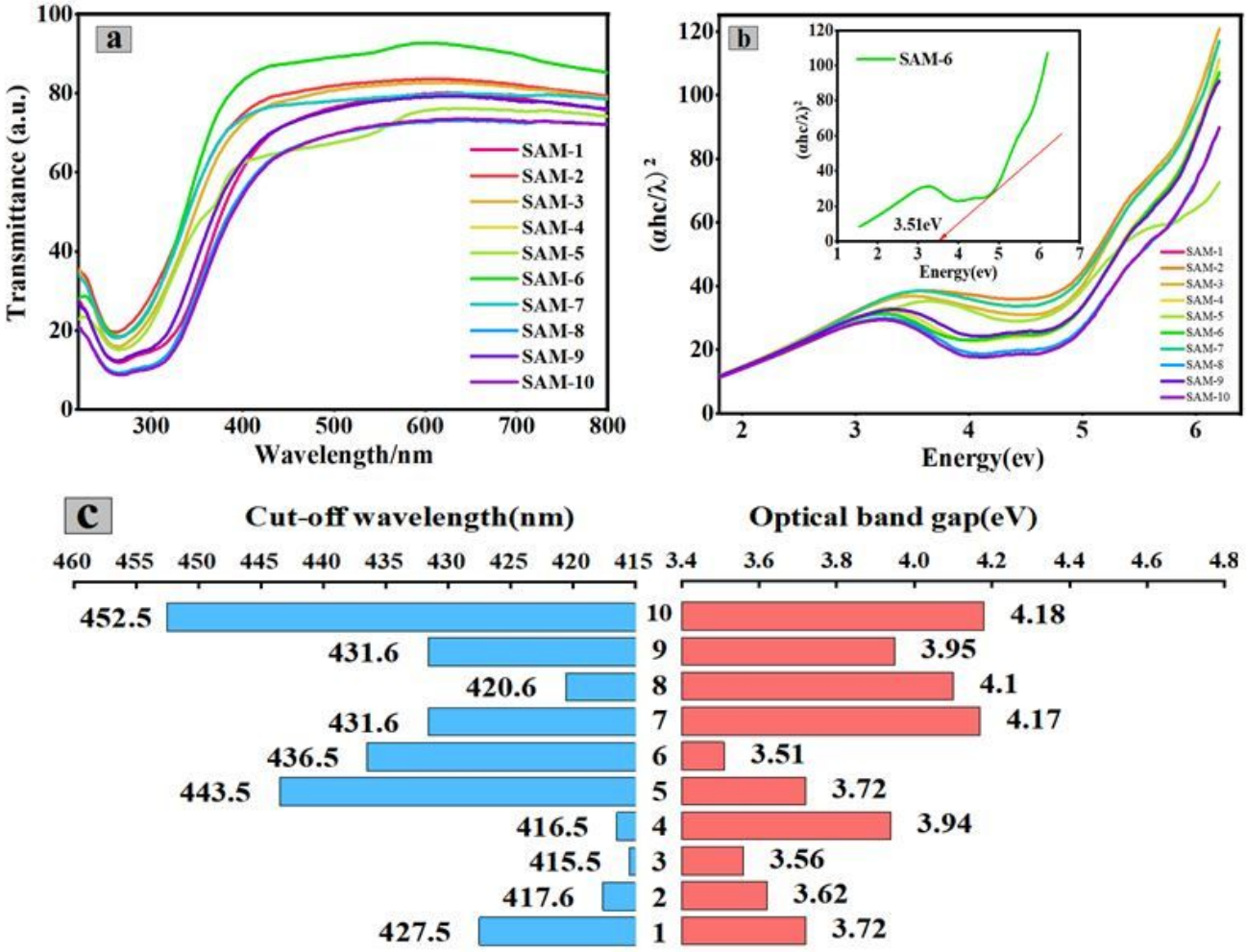

Figure 3

(a) Optical transmittance of glass doped with different amounts of TiO2 and CeO2, (b) linear fitting graph of different samples doped with TiO2 and CeO2, and (c) cut-off wavelength of optical band gap of glass doped with different amounts of TiO2 and CeO2.

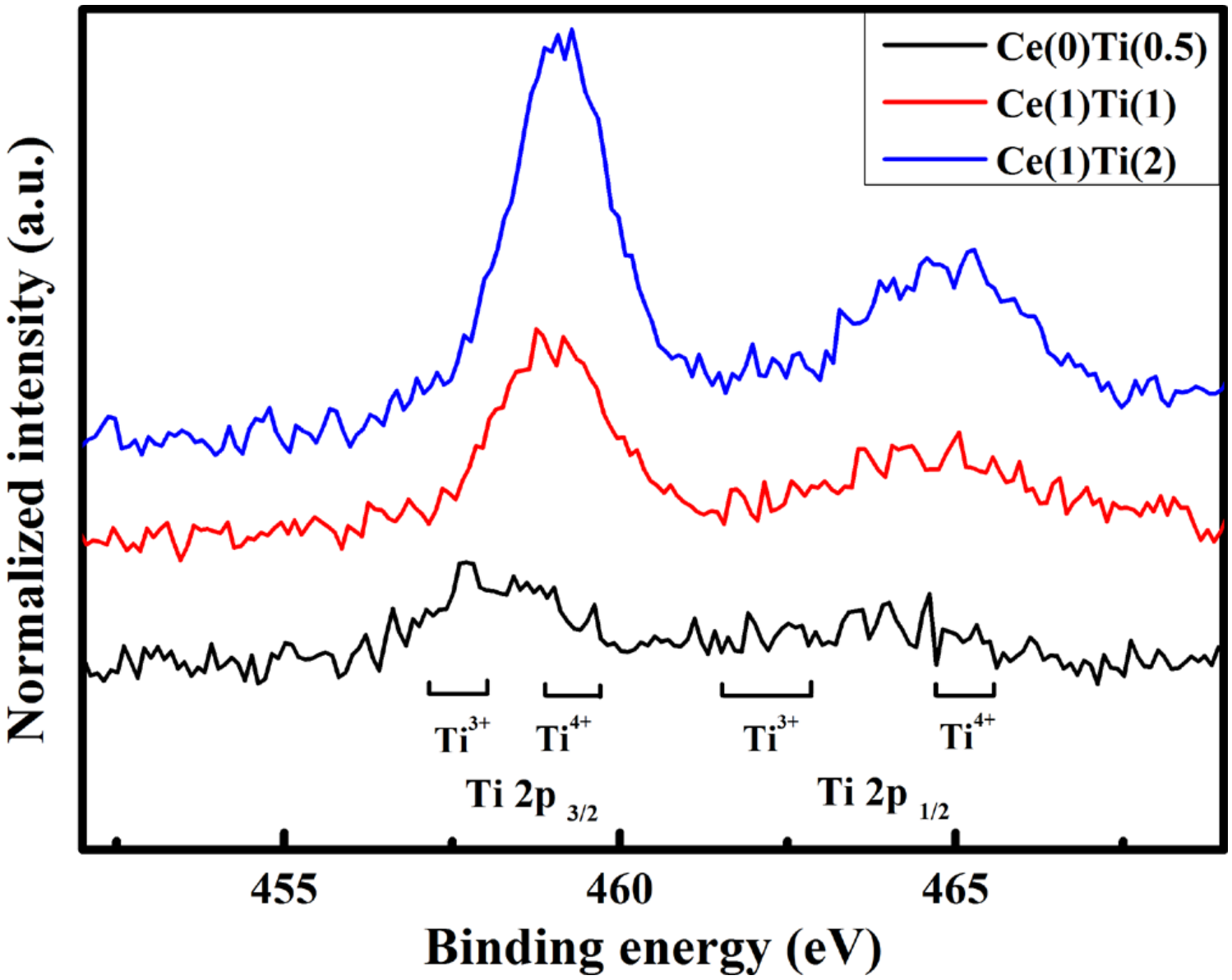

Figure 4

XPS profiles of representative glasses doped with different amounts of TiO2 and CeO2

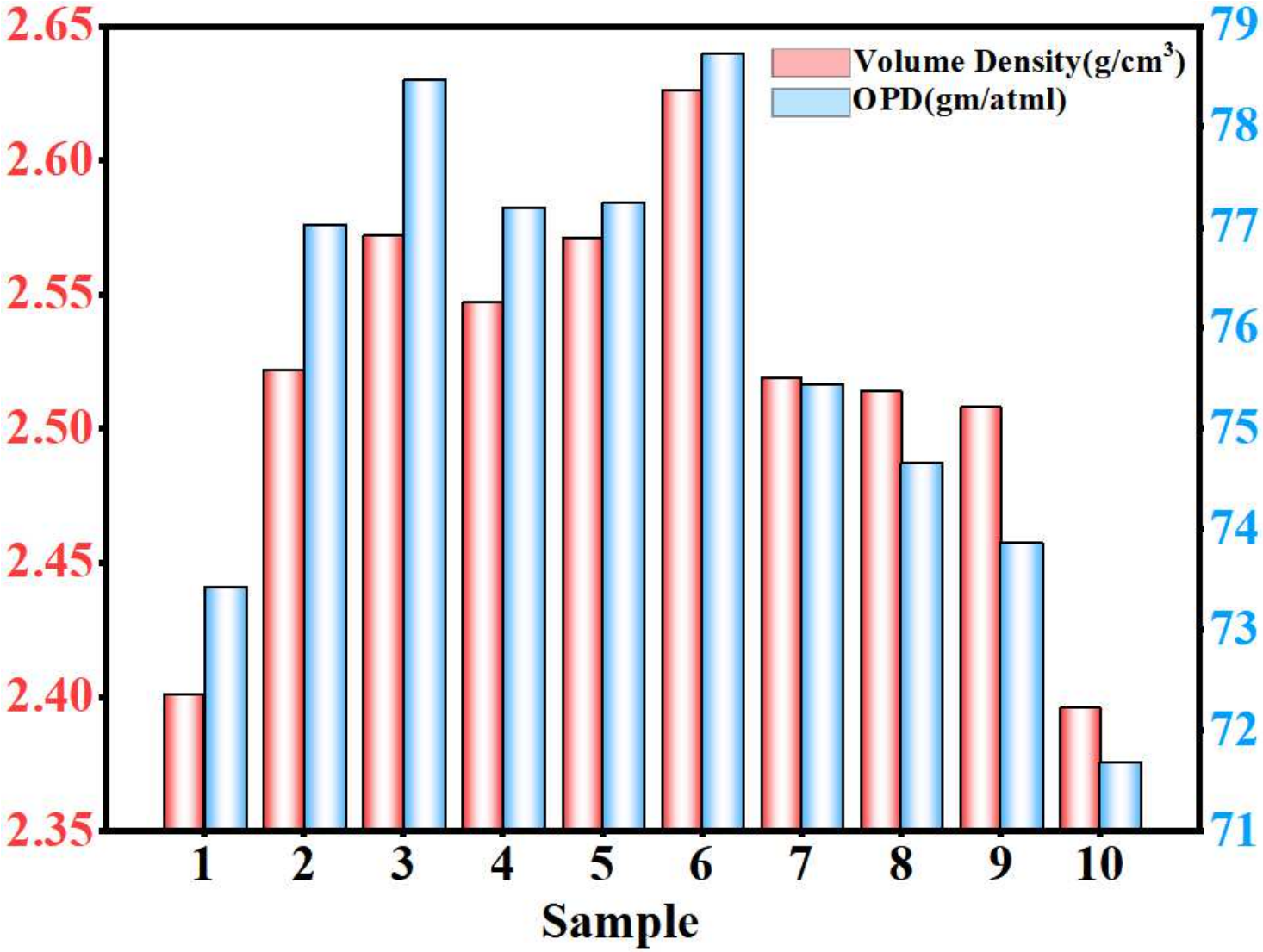

Figure 5

Volume and oxygen packing densities of glass doped with different amounts of TiO2 and CeO2

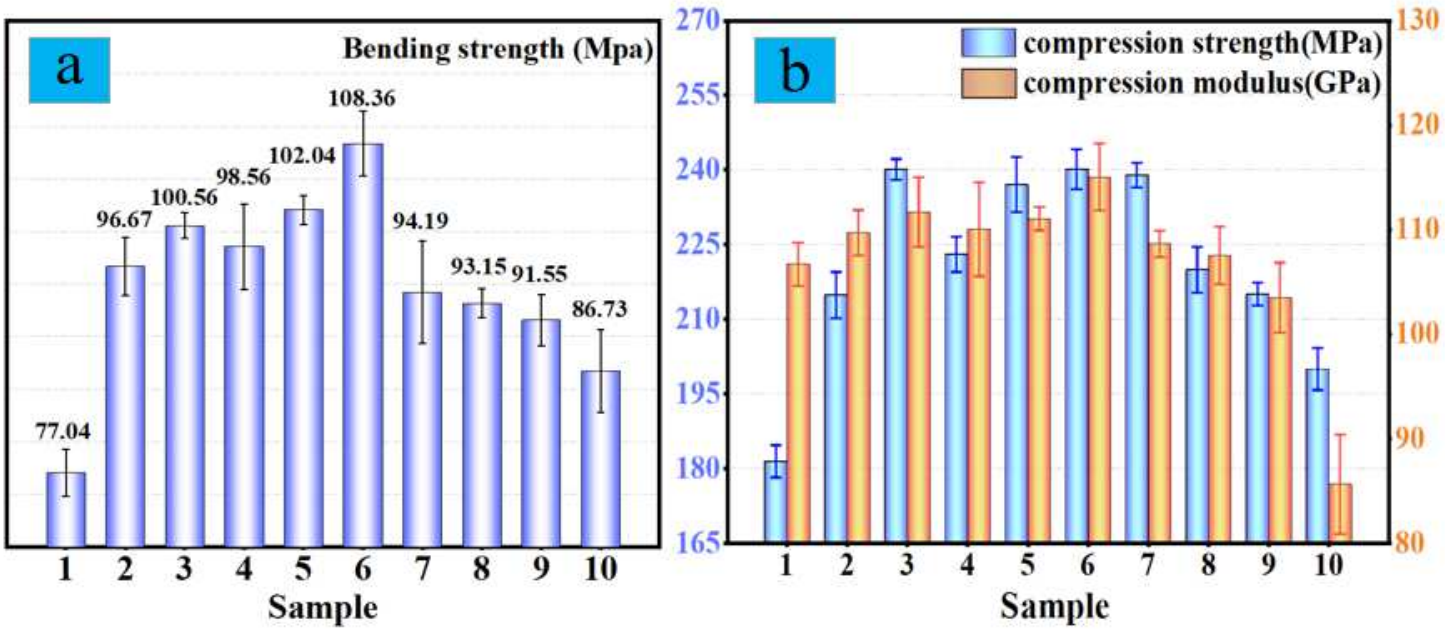

Figure 6

(a) The bending strength of glass doped with different amounts of TiO2 and CeO2, and (b) the compressive strength and modulus of glass doped with different amounts of TiO2 and CeO2